

Deep Source-Seekers with Obstacle Avoidance: Adaptive Hybrid Control with Transformers In-The-Loop

Xiyuan Zhang

University of California, San Diego, USA

xiz105@ucsd.edu

Regina Talonia

National Polytechnic Institute, Mexico

RTALONIAM1800@ALUMNO.IPN.MX

Daniel E. Ochoa

University of California, Santa Cruz, USA

DOCHOATAMAYO@UCSC.EDU

Jorge I. Poveda

*University of California, San Diego, USA**

POVEDA@UCSD.EDU

Editors: N. Ozay, L. Balzano, D. Panagou, A. Abate

Abstract

Autonomous signal source localization is a cornerstone of modern robotics, underpinning critical applications in environmental monitoring, search and rescue, and industrial automation. Traditional source-seeking methods, such as gradient-based algorithms and potential field-based approaches, often struggle with local minimum entrapment in environments cluttered with obstacles. To address these challenges, in this paper we introduce a novel model-free approach that combines a perception-driven hybrid controller—integrating adaptive continuous-time and discrete-time feedback—with an Environmental Complexity Adapter (ECA) for perception model selection. The proposed dynamics implement real-time exploration/exploitation mechanisms and complementary deep learning-based perception architectures: YOLOv10 for rapid and accurate object detection in clear conditions, and Real-Time DEtection TRansformer (RT-DETR) for enhanced robustness in noisy environments. By continuously assessing the quality of sensor data, the ECA dynamically switches between these models, optimizing the trade-off between processing speed and detection reliability. This approach harnesses the robustness of hybrid controllers while enabling efficient, perception-guided source-seeking and obstacle avoidance in complex environments. Extensive numerical simulations validate the effectiveness of the proposed approach.

Keywords: Source Seeking, Obstacle Avoidance, Hybrid Control, Transformer, Machine Learning

1. Introduction

The ability to autonomously locate signal sources is fundamental for robotic systems, with critical applications in environmental monitoring, search and rescue, and industrial automation. Source-seeking algorithms guide agents toward signal origins—such as chemical plumes, heat signatures, or sound waves—using sensory inputs. These algorithms enable robots to perform vital tasks like detecting gas leaks (Russell, 1999; Francis et al., 2022), locating survivors in disaster zones (Murphy, 2004; Azzolini et al., 2020), and monitoring pollution levels (Lilienthal and Duckett, 2004; Lewis and Bhaganagar, 2021). When deploying source-seeking robots in practice, obstacles not only present physical barriers but can also distort signal fields, complicating the localization task (Moravec, 1983). Several studies have integrated obstacle avoidance strategies using techniques

* This work was supported in part by NSF grant ECCS CAREER 2305756 and AFOSR grant FA9550-22-1-0211.

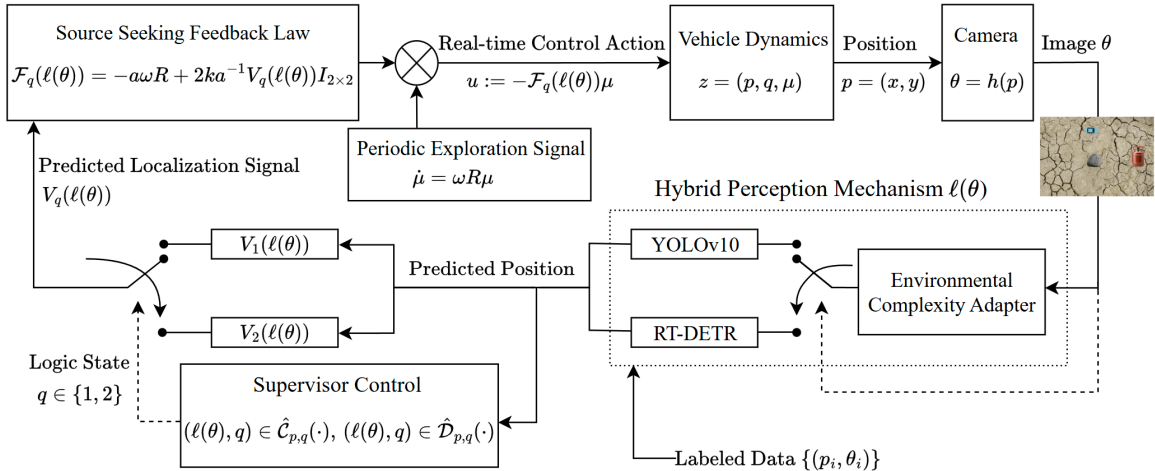


Figure 1: Closed-loop control system for source seeking and obstacle avoidance. Image data $\theta = h(p)$, captured by the *Camera* at position $p = (x, y)$, is processed by the *Hybrid Perception Mechanism* $\ell(\theta)$ (detailed in Fig. 3), which dynamically switches between *YOLOv10* for rapid detection and *RT-DETR* for robust performance under noise.

like potential field methods (Khatib, 1986) and reactive control schemes (Fox et al., 1997). Despite these advances, issues such as entrapment in local minima (Ge and Cui, 2002), computational inefficiency (LaValle, 2006), and difficulties in adapting to dynamic or uncertain environments persist (Fox et al., 1999). These challenges emphasize the need for more robust and adaptable control strategies (Siegwart et al., 2011). Motivated by the above challenges, this paper addresses perception-based source-seeking with obstacle avoidance, where a vehicle navigates toward a signal source using only signal intensity measurements while avoiding collisions. Obstacles often create non-contractible subspaces incompatible with robust global stabilization via continuous, discontinuous, or time-varying feedback (Bhat and Bernstein, 2000; Mayhew and Teel, 2011; Abdelgalil and Poveda, 2024). To overcome this, we introduce a hybrid gradient-free source-seeking controller that combines deep-learning-based perception with stability guarantees. Unlike traditional averaging-based source-seeking methods relying solely on real-time feedback (Zhang et al., 2007; Cochran and Krstic, 2009; Poveda et al., 2021; Todorovski and Krstic, 2023), our approach integrates pre-trained perception maps into the feedback loop for real-time localization using cameras for the purpose of navigation. The integration of perception maps with hybrid controllers for obstacle avoidance was first investigated in (Murillo-Gonzalez and Poveda, 2022), where convolutional neural networks were utilized. The combination of reinforcement learning with hybrid control strategies has been recently explored in works such as (De Priester et al., 2022, 2024). However, to the best of our knowledge, real-time adaptive hybrid control using transformer-based architectures remains an open problem. In this work, we propose a novel model-free approach that combines transformer networks with extremum-seeking control for real-time source-seeking in autonomous systems, where the gradient of the localization objective is learned online. An overview of the system is illustrated in Fig. 1. A key feature is the Environmental Complexity Adapter (ECA), based on VGGNet (Simonyan and Zisserman, 2015), which selects between YOLOv10 (Wang et al., 2024) for fast detection in clear environments and RT-DETR (Zhao et al., 2024) for robust detection in noisy or occluded conditions. By incorporating visual transformers, the system addresses challenges

in complex environments where traditional recurrent neural networks fail. Enabled by a hybrid dynamical systems framework (Goebel et al., 2012), our approach ensures robust interconnections between feedback laws and perception mechanisms, guaranteeing safe and reliable navigation. To the best of our knowledge, this is the first framework to incorporate online real-time hybrid source-seeking control with offline-trained deep learning perception models, within a framework grounded in averaging theory and equipped with formal stability guarantees.

The rest of the paper is organized as follows. Section 2 introduces the preliminaries. Section 3 formulates and derives the dynamics that integrate source seeking and obstacle avoidance. Section 4 presents the architecture of the Hybrid Perception Mechanism, highlighting the role of the ECA. Finally, Section 5 presents numerical results, demonstrating performance in environments modeled with real-world images.

2. Preliminaries

Notation: We denote the Manhattan (L1-norm) of a vector $z \in \mathbb{R}^n$ by $\|z\|_1$, and the Euclidean (L2-norm) of a vector $z \in \mathbb{R}^n$ by $\|z\|_2$. We define the minimum distance from $z \in \mathbb{R}^n$ to a closed set $\mathcal{A} \subset \mathbb{R}^n$ as $|z|_{\mathcal{A}} := \min_{s \in \mathcal{A}} \|z - s\|_2$. Given $x, y \in \mathbb{R}^n$ we use $(x, y) = [x^\top, y^\top]^\top$ for their concatenation. The unit circle in \mathbb{R}^2 is denoted by $\mathbb{S}^1 := \{z \in \mathbb{R}^2 : z_1^2 + z_2^2 = 1\}$. For any $r > 0$, we use $r\mathbb{B}$ to denote the closed ball of radius r centered at the origin. For a point $p \in \mathbb{R}^n$ and $r > 0$, the closed ball of radius r centered at p is defined via the Minkowski sum as $p + r\mathbb{B} := \{x \in \mathbb{R}^n : \|x - p\|_2 \leq r\}$. For any set C , we denote its closure by \overline{C} . A set-valued map $F : \mathbb{R}^n \rightrightarrows \mathbb{R}^n$ is said to be outer semicontinuous if its graph $\text{gph } F = \{(x, f) \in \mathbb{R}^n \times \mathbb{R}^n : f \in F(x)\}$ is closed. It is said to be locally bounded if for all $x \in \mathbb{R}^n$ there exists a neighborhood $V \ni x$ such that $F(V) = \bigcup_{y \in V} F(y)$ is bounded.

To model our algorithms, we employ hybrid dynamical systems (HDS) that incorporate continuous-time and discrete-time evolution. Specifically, an HDS with state $z \in \mathbb{R}^n$ is represented by its data $\mathcal{H} := \{C, F, D, G\}$ and the dynamics

$$z \in C, \quad \dot{z} \in F(z), \tag{1a}$$

$$z \in D, \quad z^+ \in G(z), \tag{1b}$$

where the set-valued mappings $F : \mathbb{R}^n \rightrightarrows \mathbb{R}^n$ and $G : \mathbb{R}^n \rightrightarrows \mathbb{R}^n$, called the flow map and the jump map, respectively, describe the evolution of the state z when it belongs to the flow set C and the jump set D , respectively. Solutions to HDS of the form (1) are defined on hybrid time domains, i.e., they are parameterized by both a continuous-time index $t \in \mathbb{R}_{\geq 0}$, and a discrete-time index $j \in \mathbb{Z}_{\geq 0}$. Accordingly, the notation \dot{z} in (1a) represents the derivative of z with respect to time t , i.e., $\frac{dz}{dt}(t, j)$; and z^+ in (1b) represents the value of z after an instantaneous jump, i.e., $z(t, j + 1)$. For a precise definition of hybrid time domains and solutions to HDS of the form (1) we refer the reader to (Goebel et al., 2012, Ch. 2).

To guarantee the well-posedness and enable robustness analysis of our algorithms, we impose the following standing assumption for the HDS considered in this paper:

Standing Assumption [Hybrid Basic Conditions] *A HDS of the form (1) is said to satisfy the hybrid basic conditions if: 1) the sets $C \subset \text{dom}(F)$ and $D \subset \text{dom}(G)$ are closed, 2) the jump map G is outer semicontinuous and locally bounded relative to D , 3) the flow map F is outer semicontinuous, locally bounded, and convex valued.*

3. Source Seeking and Obstacle Avoidance via Hybrid Control

In this paper, we address the source-seeking problem for a planar robot navigating through an environment with obstacles using cameras for the purpose of position feedback. We consider a robot with position coordinates $p = (x, y) \in \mathbb{R}^2$ and dynamics $\dot{p} = u$, where $u \in \mathbb{R}^2$ denotes the velocity control input. We aim to synthesize a robust and gradient-free feedback control law u that accomplishes two objectives: 1) driving the robot to a neighborhood of $\operatorname{argmax} J$, where $J : \mathbb{R}^2 \rightarrow \mathbb{R}$ is an unknown but measurable potential field, and 2) ensuring collision avoidance with respect to a predefined obstacle set \mathcal{N} . For the purpose of analysis, we make the following assumptions on the potential function J and the obstacle:

Assumption 1 *The potential function $J : \mathbb{R}^2 \rightarrow \mathbb{R}_{\geq 0}$ is continuously differentiable, $-J$ is radially unbounded, and the set $\mathcal{A}_J := \{p^* \in \mathbb{R}^2 : J(p^*) \geq J(p), \forall p \in \mathbb{R}^2\}$, is not empty.*

Assumption 2 *There exists $\rho \in \mathbb{R}_{>0}$ and $\delta \in \mathbb{R}_{>0}$, such that the obstacle $\mathcal{N} \subset \mathbb{R}^2$ satisfies $\mathcal{N} \subset p_0 + \rho\mathbb{B}$ and $(p_0 + \rho\sqrt{2}\mathbb{B}) \cap (\mathcal{A}_J + \delta\mathbb{B}) = \emptyset$, where $p_0 = (x_0, y_0) \in \mathbb{R}^2$.*

3.1. Operational Space

To achieve global obstacle avoidance, we employ a covering of the operational space constructed as follows. For each $p_0 \in \mathbb{R}^2$ and $\rho > 0$, define the set $\mathcal{B}_{p_0, \rho} := \{p \in \mathbb{R}^2 : \|p - p_0\|_1 \leq \rho\sqrt{2}\}$, which satisfies $p_0 + \rho\mathbb{B} \subset \mathcal{B}_{p_0, \rho} \subset p_0 + \rho\sqrt{2}\mathbb{B}$. Following a similar space-covering construction presented in (Sanfelice et al., 2006; Poveda et al., 2021), we define the following auxiliary sets:

$$\begin{aligned} \mathcal{L}_{1a} &:= \left\{p \in \mathbb{R}^2 : y < -x + y_0 + x_0 - \rho\sqrt{2}\right\}, \quad \mathcal{L}_{1b} := \left\{p \in \mathbb{R}^2 : y < x + y_0 + x_0 - \rho\sqrt{2}\right\}, \\ \mathcal{L}_{2a} &:= \left\{p \in \mathbb{R}^2 : y > x + y_0 + x_0 + \rho\sqrt{2}\right\}, \quad \mathcal{L}_{2b} := \left\{p \in \mathbb{R}^2 : y > -x + y_0 + x_0 + \rho\sqrt{2}\right\}. \end{aligned}$$

Additionally, we define the virtual sets $\mathcal{O}_1 := \mathcal{L}_{1a} \cup \mathcal{L}_{1b}$, $\mathcal{O}_2 := \mathcal{L}_{2a} \cup \mathcal{L}_{2b}$, $\mathcal{O} := \mathcal{O}_1 \cup \mathcal{O}_2$. Then, the obstacle-free region can be defined as $\mathcal{O} = \mathbb{R}^2 \setminus \mathcal{B}_{p_0, \rho}$. By construction, the obstacle \mathcal{N} satisfies $\mathcal{N} \cap \mathcal{O} = \emptyset$, meaning \mathcal{N} does not intersect any of the sets \mathcal{O}_i for $i \in \{1, 2\}$, and the set of global maximizers satisfies $\mathcal{A}_J \subseteq \mathcal{O}_1 \cap \mathcal{O}_2$.

3.2. Localization Function

For each of the sets \mathcal{O}_1 and \mathcal{O}_2 , we design a suitable localization function V_q , where $q \in \{1, 2\}$, to enable the robot to locate the source of the potential field J . These functions are given by:

$$V_q(p) := \begin{cases} J_q(p) - \hat{J}(p), & \forall p \in \mathcal{O}_q, \\ \infty, & \forall p \notin \mathcal{O}_q \end{cases}, \quad \text{with } q \in \{1, 2\}, \quad (2)$$

where \hat{J} denotes the robot's measurement of the intensity of the potential field J , and J_q represents a virtual barrier signal defined only on each set \mathcal{O}_q . We consider localization functions V_q that satisfy the following assumption borrowed from Sanfelice et al. (2006) and Poveda et al. (2021).

Assumption 3 *Let $W_q := V_q + J^*$. The hybrid localization functions $\{V_q\}_{q \in \{1, 2\}}$ satisfy the following: 1) For each $q \in \{1, 2\}$, there exist functions $\alpha_{1,q}, \alpha_{2,q} \in \mathcal{K}_{\infty}$, and proper indicators $\tilde{\omega}_q$ of \mathcal{A}_J on \mathcal{O}_q , such that $\alpha_{1,q}(\tilde{\omega}_q(p)) \leq W_q(p) \leq \alpha_{2,q}(\tilde{\omega}_q(p)), \forall p \in \mathcal{O}_q$. 2) For each $q \in \{1, 2\}$, we have $Z_{\nabla W_q} = \{p^* \in \mathcal{O}_q : \nabla W_q(p^*) = 0\} = \mathcal{A}_J$, where \mathcal{A}_J is defined in Assumption 1. 3) For each $q \in \{1, 2\}$, the function $V_q(p)$ is continuously differentiable in \mathcal{O}_q .*

When $\hat{J} = J$, and J satisfies Assumption 1, we can readily satisfy the conditions in Assumption 3 by selecting compatible barrier functions J_q . For instance, we can construct J_q as follows:

$$J_q(p) := B\left(|p|_{\mathbb{R}^2 \setminus \mathcal{O}_q}^2\right), \quad B(s) := \begin{cases} (s - \rho)^2 \log\left(\frac{1}{s}\right), & \text{if } s \in [0, \rho], \\ 0 & \text{if } s > \rho \end{cases}, \quad (3)$$

where $\rho \in (0, 1]$ is a sufficiently small tunable parameter.

3.3. Hybrid Gradient-Free Source-Seeking Controller

To discover the position of the source in real-time, while simultaneously avoiding the obstacle, we consider a hybrid gradient-free source-seeking controller. The controller has state $\zeta = (q, \mu) \in \{1, 2\} \times \mathbb{S}^1$, where q is a logic state, and μ is an auxiliary state whose behavior will be detailed below, and the control action is denoted by $u \in \mathbb{R}^2$. Taking measurements of the robot's position $p \in \mathbb{R}^2$, the continuous-time dynamics of the controller are defined as follows:

$$\dot{\zeta} = \begin{pmatrix} \dot{q} \\ \dot{\mu} \end{pmatrix} = F_c(\zeta) = \begin{pmatrix} 0 \\ \omega R \mu \end{pmatrix}, \quad (4)$$

and the real-time control action is given by $u = -\mathcal{F}_q(p)\mu$, where $\mathcal{F}_q : \mathbb{R}^2 \rightarrow \mathbb{R}^2$ is defined by:

$$\mathcal{F}_q(p) = -a\omega R + 2ka^{-1}V_q(p)I_{2 \times 2}, \quad R := \begin{bmatrix} 0 & 1 \\ -1 & 0 \end{bmatrix}, \quad (5)$$

for all $p \in \mathbb{R}^2$, with tunable parameters $a, \omega, k \in \mathbb{R}_{>0}$. Given the dynamics of μ in (4) and the definition of R , during flows, μ evolves as a periodic oscillatory signal which can be explicitly expressed as:

$$\mu(t) = \exp(\omega Rt)\mu(0) = \begin{bmatrix} \cos(\omega t) & \sin(\omega t) \\ -\sin(\omega t) & \cos(\omega t) \end{bmatrix} \begin{bmatrix} \mu_1(0) \\ \mu_2(0) \end{bmatrix}. \quad (6)$$

Since $\frac{d}{dt}(\mu^\top \mu) = 0$, it follows that \mathbb{S}^1 is forward invariant for any $\omega > 0$. The controller employs the periodic behavior of μ to dither and estimate, in real-time, the gradients of the localization functions $\{V_q\}_{q \in \{1, 2\}}$.

To ensure convergence to the signal source while avoiding local minima of the potential function J , we incorporate discrete switching of the logic state q via the discrete-time dynamics:

$$\zeta^+ = G_c(\zeta) = \begin{pmatrix} 3 - q \\ \mu \end{pmatrix}. \quad (7)$$

The interconnection between the hybrid gradient-free controller described in (4)-(7), and the vehicle dynamics $\dot{p} = u$ lead to a closed-loop HDS of the form (1) with state $z = (p, q, \mu) \in \mathbb{R}^2 \times \{1, 2\} \times \mathbb{S}^1$, and data $\mathcal{H} = (C, F, D, G)$, where

$$\dot{z} = F(z) := \{-\mathcal{F}_q(p)\mu\} \times \{F_c(q, \mu)\}, \quad z \in C_z = C_{p,q} \times \mathbb{S}^1, \quad (8a)$$

$$z^+ = G(z) := \{p\} \times \{G_c(q, \mu)\}, \quad z \in D_z = D_{p,q} \times \mathbb{S}^1. \quad (8b)$$

The sets $C_{p,q}$ and $D_{p,q}$ are respectively defined by:

$$C_{p,q} := \{(p, q) \in \overline{\mathcal{O}} \times \{1, 2\} : V_q(p) \leq \chi V_{3-q}(p)\}, \quad (9a)$$

$$D_{p,q} := \{(p, q) \in \overline{\mathcal{O}} \times \{1, 2\} : V_q(p) \geq (\chi - \lambda) V_{3-q}(p)\}, \quad (9b)$$

where $\chi > 0$ and $\lambda > 0$ are tunable parameters that satisfy $\chi - \lambda > 1$. These parameters induce hysteresis in the switching mechanism and preclude Zeno behavior. The HDS induced by the data \mathcal{H} in (8) satisfies the standing assumption.

Building on the robustness of this nominal HDS induced by \mathcal{H} , the following sections develop its interconnection with transformer-based perception architectures for real-time position estimation.

4. Deep Learning-based Hybrid Perception Mechanism

Adaptive seeking dynamics of the form (8) have been studied using averaging theory in the literature under the assumption that the vehicle has access to measurements of its position at all times Poveda et al. (2021). However, in practical settings, vehicles navigate using perception-based mechanisms that leverage images and videos from cameras. In this work, we augment the nominal HDS induced by \mathcal{H} through the incorporation of visual perception mechanisms for state estimation from image data. Building on the perception model structure introduced in (Dean et al., 2020), we introduce a Hybrid Perception Mechanism ℓ that maps camera images $\theta = h(p)$ to position estimates via $\ell(\theta) = Mp + e(p)$, where $M \in \mathbb{R}^{2 \times 2}$ is a constant transformation matrix and $e(p)$ denotes the measurable perception approximation error generated by the Hybrid Perception Mechanism. This mechanism serves as a crucial bridge between raw visual information and the robot's decision-making system, leading to the perception-based control law:

$$u := -\mathcal{F}_q(\ell(\theta))\mu = (-a\omega R + 2ka^{-1}V_q(\ell(\theta))I_{2 \times 2})\mu. \quad (10)$$

The mechanism is learned through data-driven techniques (see Section 4.2), utilizing a dataset of labeled images and corresponding robot position, denoted as $T = \{(p_i, \theta_i)\}_{i=1}^N$. Similar to (Dean et al., 2020), it is assured to satisfy the following assumption.

Assumption 4 For each compact set $K \subset \mathbb{R}^2$, and each pair $L, \varepsilon > 0$, there exists a function ℓ learned with training data $T = \{(p_i, \theta_i)\}_{i=1}^N$, such that $K \subset \text{int}(S_\varepsilon^L)$, where $S_\varepsilon^L := \bigcup_{(p_d, \theta_d) \in T} \{p \in p_d + r\mathbb{B} : \|\ell(\theta_d) - Mp_d\|_2 + L\|p - p_d\|_2 \leq \varepsilon\}$.

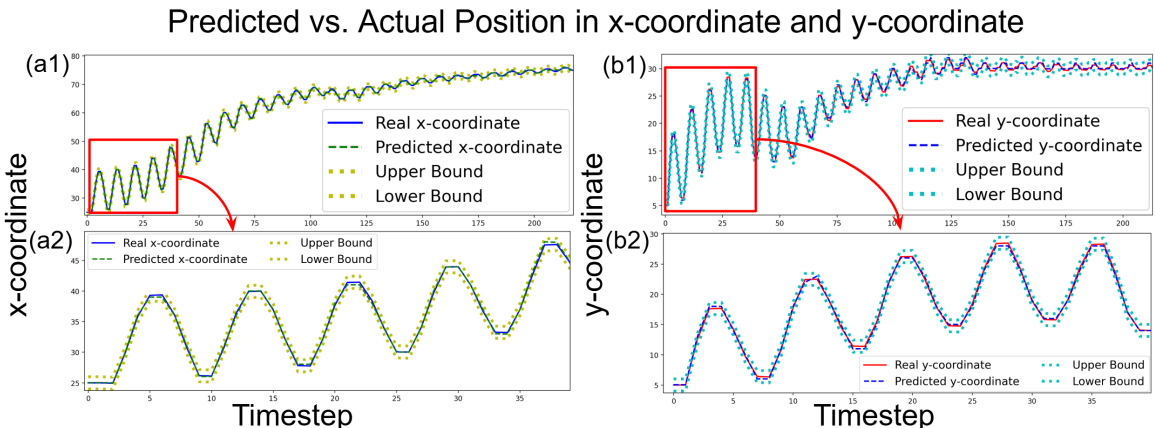


Figure 2: Comparison of predicted vs. actual vehicle positions in (a1) the x -coordinate and (b1) y -coordinate, with (a2) and (b2) providing zoomed-in views. The oscillatory behavior is characteristic of seeking dynamics that implement real-time periodic dithering.

In words, Assumption 4 states that the Hybrid Perception Mechanism can approximate the robot's position with sufficiently high accuracy across the region of interest. Specific examples of how to realize these mechanisms using transformers will be discussed in Section 4.2.

The following technical lemma is key for our results:

Lemma 1 *Let $F(p) := (\ell \circ h)(p) - Mp$, and suppose that Assumption 4 holds and $p \mapsto F(p)$ is L -Lipschitz. Then, $\|\ell(\theta) - Mp\|_2 \leq \varepsilon$, for all (p, θ) such that $p \in \mathcal{S}_\varepsilon^L$.*

Figure 2 illustrates Lemma 1 on a sample trajectory of the closed-loop HDS. As observed, the predictions of the robot position remain consistent in an ε -neighborhood of the real trajectory, so we can consider taking $M = I$ for our later computation of the perception approximation-error.

4.1. Main Stability Result

Following Lemma 1, the perception-based closed-loop HDS, which we denote as $\hat{\mathcal{H}}$, uses the predicted position $\ell(\theta) = (\ell \circ h)(p)$ and operates as a perturbed system where the adaptive continuous-time dynamics of the robot's position are given by:

$$\dot{p} = -\mathcal{F}_q(\ell(\theta))\mu = -\mathcal{F}_q(Mp + e(p))\mu, \quad \forall p \in \mathcal{S}_\varepsilon^L, \quad (11)$$

and $e : \mathbb{R}^2 \supset \text{dom}(e) \rightarrow \varepsilon\mathbb{B}$ is the measurable perception approximation-error, caused by the Hybrid Perception Mechanism. Accordingly, by using (8), we can represent the flows of the HDS $\hat{\mathcal{H}}$ as follows:

$$\dot{z} = \hat{F}(z) = \begin{pmatrix} -\mathcal{F}_q(\ell(\theta))\mu \\ 0 \\ \omega R\mu \end{pmatrix}, \quad z \in \hat{C} := \hat{C}_{p,q} \times \mathbb{S}^1. \quad (12a)$$

Similarly, the discrete-time dynamics of the HDS $\hat{\mathcal{H}}$, that cause the logic state q to transition between modes, are given by:

$$z^+ = \hat{G}(z) = \begin{pmatrix} p \\ 3-q \\ \mu \end{pmatrix}, \quad z \in \hat{D} := \hat{D}_{p,q} \times \mathbb{S}^1. \quad (12b)$$

The sets $\hat{C}_{p,q}$ and $\hat{D}_{p,q}$ are defined from (9) by replacing the actual position p with the output of the Hybrid Perception Mechanism $\ell(\theta)$:

$$\hat{C}_{p,q} := \{(\ell(\theta), q) \in \overline{\mathcal{O}} \times \{1, 2\} : V_q(\ell(\theta)) \leq \chi V_{3-q}(\ell(\theta))\}, \quad (12c)$$

$$\hat{D}_{p,q} := \{(\ell(\theta), q) \in \overline{\mathcal{O}} \times \{1, 2\} : V_q(\ell(\theta)) \geq (\chi - \lambda) V_{3-q}(\ell(\theta))\}. \quad (12d)$$

The following theorem presents the main theoretical result of this paper. Its proof is omitted due to space constraints.

Theorem 1 *Suppose that Assumptions 1–4 hold. Then, for any compact set $K_0 \subset \mathbb{R}^2 \setminus \mathcal{B}_{p_0, \rho}$ and each precision value $\delta \in \mathbb{R}_{>0}$, we can find $a^* \in \mathbb{R}_{>0}$, such that for each $a \in (0, a^*)$ there exists a frequency-threshold $\omega^* \in \mathbb{R}_{>0}$, such that for each $\omega > \omega^*$ there exists an error-bound $\varepsilon^* \in \mathbb{R}_{\geq 0}$ such that for each complete solution $z = (p, q, \mu)$ to the perception-based HDS $\hat{\mathcal{H}}$ with perception approximation-error e bounded by ε^* , and initial condition $p(0, 0) \in K_0$ it follows that:*

- i) Source Seeking: $p(t, j)$ converges to $\mathcal{A}_J + (\delta + a)\mathbb{B}$ in finite time;
- ii) Obstacle Avoidance: $p(t, j) \notin \mathcal{N}$ for all $(t, j) \in \text{dom}(z)$.

□

4.2. Robot Coordinates Detection and Environmental Complexity Adapter

To enhance perception accuracy during source seeking, Lemma 1 ensures that the perception approximation error e remains within a threshold ε . To minimize e while balancing accuracy and computational efficiency, we propose a *Hybrid Perception Mechanism* (Fig. 3) with a dual-model approach, integrating YOLOv10 with the Transformer-based RT-DETR. The *Environmental Complexity Adapter* (ECA) (shown on the left side of Fig. 3), generalized from VGG networks (Simonyan and Zisserman, 2015), outputs a binary adapter vector $\mathbf{a} \in \{(0, 1), (1, 0)\}$ to enable model selection based on each perception frame.

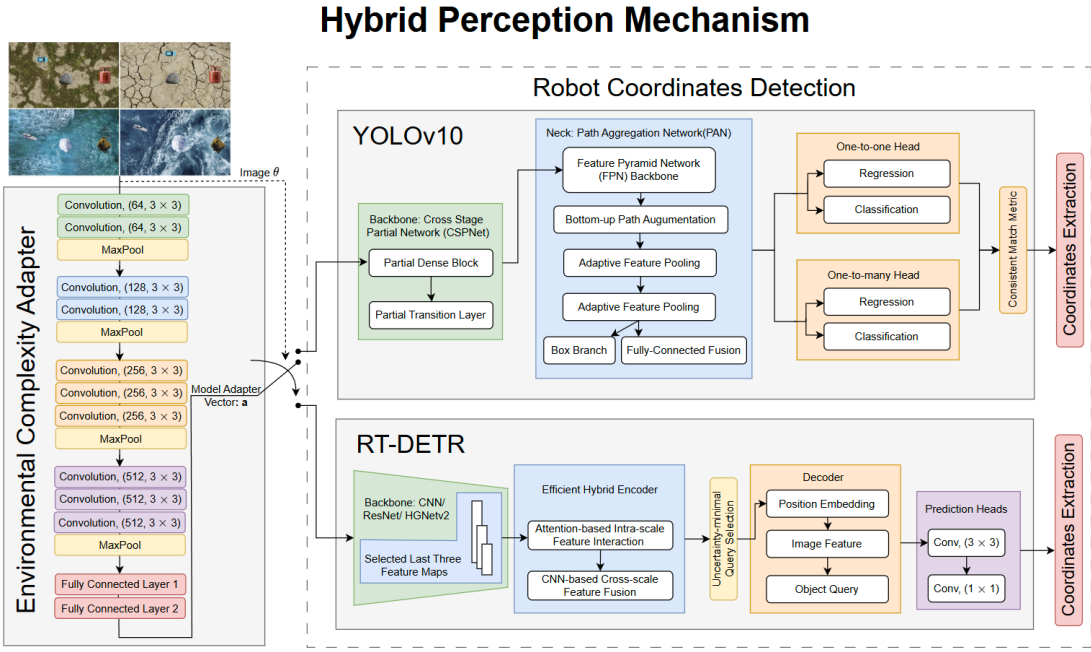


Figure 3: The Environmental Complexity Adapter (ECA) generates an adapter vector \mathbf{a} to guide model selection. Only the model associated with an adapter value of 1 is activated, adaptively selecting YOLOv10 for speed or RT-DETR for robustness in complex scenes. The outputs of the Hybrid Perception Mechanism are the predicted coordinates of the robot.

The ECA vector dynamically switches between two models: YOLOv10 (Wang et al., 2024) for high-speed detection in clean environments and RT-DETR (Zhao et al., 2024) for robust performance in complex background scenarios. YOLOv10, the latest version of the YOLO object detection networks, employs a deep architecture for enhanced precision, ideal for real-time applications requiring rapid environmental assessments. In contrast, Transformer-based models, such as RT-DETR, leverage self-attention mechanisms for neighboring-scene understanding and excel in handling complex, multi-object environments. RT-DETR improves upon traditional DETR (Zhu et al., 2021) by incorporating an encoder with convolutional and multi-scale feature processing, achieving improved accuracy in complex-environment deployment.

In Table 1, we show that the ECA architecture is the core component of the Hybrid Perception Mechanism, and dynamically balances the trade-offs between YOLOv10's speed (the shortest inference time 14.33 ms) and RT-DETR's accuracy (the best root mean square error (RMSE)

Evaluation Metric	YOLOv10	RT-DETR	Hybrid Perception Mechanism
RMSE	0.53	0.11	0.28
Average Inference Time (ms)	14.33	40.52	23.45

Table 1: The Root Mean Square Error (RMSE) of the perception coordinates and the average inference time per frame during testing for YOLOv10 and RT-DETR are compared against our proposed Hybrid Perception Mechanism under the environment setting shown in Fig. 4(a).

0.11) based on real-time environmental complexity. Using a VGGNet-inspired backbone, the ECA evaluates factors such as noise, occlusion, and background variability to switch models accordingly: YOLOv10 is deployed for low-complexity scenarios requiring rapid inference, while RT-DETR handles high-complexity environments with robust global context modeling. This adaptability achieves a balanced RMSE and inference time, optimizing detection performance and enabling reliable navigation across diverse conditions.

5. Numerical and Experimental Results

The autonomous system is simulated in a 2D grid-based environment of size 60×100 pixels (height \times width), with the origin located at the top-left corner (Fig. 4). The robot, modeled as a transport entity (e.g., a land vehicle or an ocean ship), starts at $p(0) = (25, 5)$ across Fig. 4(a) to (d). Obstacles are stationary entities, such as rocks or icebergs, represented by a circular obstacle centered at $(50, 30)$ with a radius of 5 pixels. The target region is modeled as a resource source centered at $(90, 30)$ with a radius of 7 pixels. Successful navigation is achieved when the robot's center reaches the target region while avoiding the obstacle. For Fig. 4, controller parameters were con-

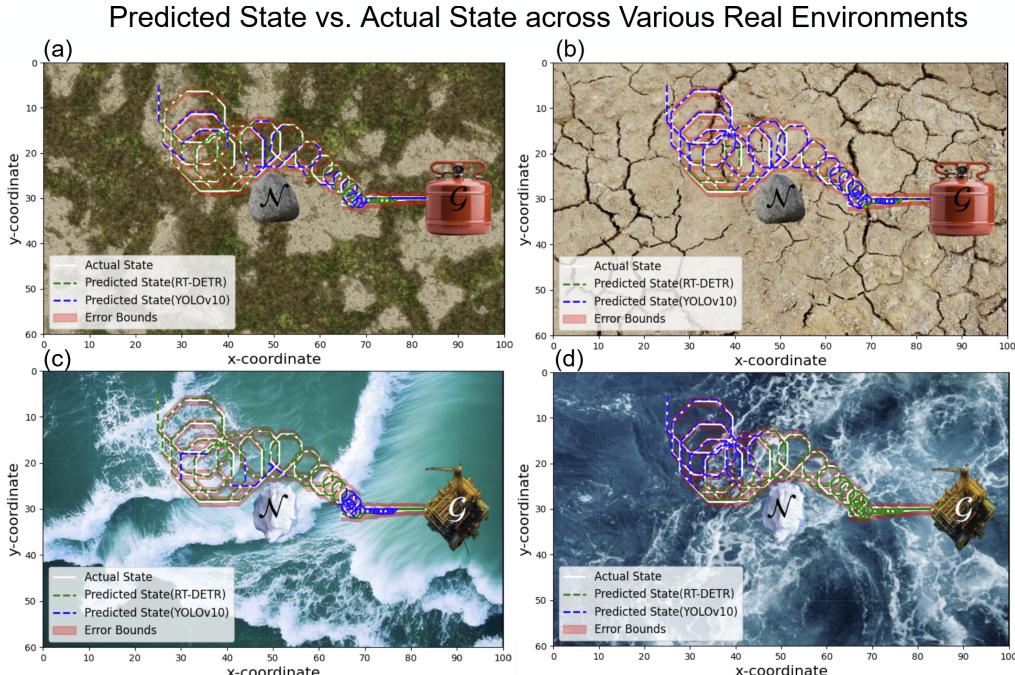


Figure 4: Across diverse real-world image backgrounds, the system dynamically selects between YOLOv10 and RT-DETR based on environmental complexity. Predicted trajectories are depicted using blue dashed lines for YOLOv10 and green dashed lines for RT-DETR.

sistent across subfigures (a) to (d) $\lambda = 0.09$, $\chi = 1.1$, $a = 0.05$, $k = 0.05$, and $\omega = 80$. We conduct the experiments with multiple real-world nonhomogeneous backgrounds to evaluate the performance of the Hybrid Perception Mechanism, demonstrating its robustness across various scenarios. As shown in Fig. 4, we test four different backgrounds: grassland, cracked land, and two ocean environments. The ECA consistently identified high-complexity areas (green trajectories by RT-DETR) and low-complexity areas (blue trajectories by YOLOv10), enabling adaptive model selection for robot coordinates detection. The robot’s trajectories closely match the predicted states of the perception-based hybrid control system, demonstrating its accuracy and robustness across various environments. Note that Zeno behavior can be precluded by tuning thresholds that trigger the switches to induce hysteresis.

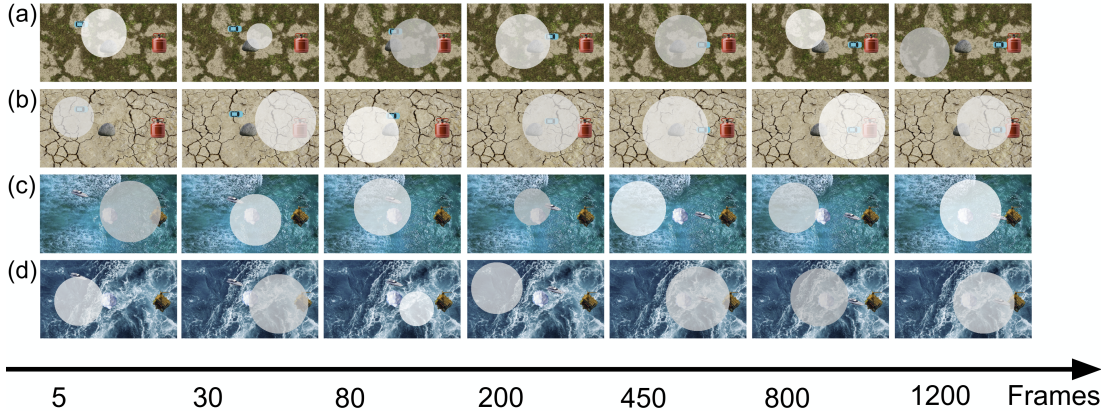


Figure 5: Snapshots of the robot trajectories under conditions of unpredictable occlusions.

To evaluate the robustness and advantages of Transformers, we introduce occlusions—modeled as translucent “bubbles” that simulate real-world noise like clouds or debris—across diverse non-homogeneous backgrounds. We characterize each occlusion as a uniform obstruction within a localized region, maintaining consistent intensity (e.g., a cloud or dust patch partially covering the camera view). Occlusion effects were introduced only during the testing stage (with no occlusions during training) to evaluate the model’s generalization capability. As shown in Fig. 5, despite unpredictable, frame-varying occlusions in nonhomogeneous backgrounds, the robot reliably reaches the target, highlighting the robustness of the Hybrid Perception Mechanism in dynamic environments.

6. Discussion and Conclusion

We propose a Hybrid Perception Mechanism that enhances robotic source-seeking by transforming sensory inputs into actionable decisions, with an Environmental Complexity Adapter (ECA) that dynamically optimizes model selection for varying environments. The ECA switches between YOLOv10 for fast detection in clear settings and RT-DETR for robustness in noisy or occluded conditions, enhancing robustness and adaptability. By integrating pre-trained perception models into an adaptive hybrid feedback loop for obstacle avoidance and source seeking, our approach overcomes fundamental limitations of traditional smooth adaptive methods that rely on real-time position feedback. The proposed approach combines deep learning with extremum seeking to learn both positions and gradients online while retaining semi-global practical stability guarantees, a first in source-seeking systems. These innovations address key challenges in source-seeking tasks, paving the way for autonomous systems that integrate tools from both control theory and machine learning.

References

- Mahmoud Abdelgalil and Jorge I Poveda. Hybrid minimum-seeking in synergistic lyapunov functions: Robust global stabilization under unknown control directions. *arXiv preprint arXiv:2408.04882*, 2024.
- Ilario A Azzolini, Nicola Mimmo, and Lorenzo Marconi. An extremum seeking approach to search and rescue operations in avalanches using arva. *IFAC-PapersOnLine*, 53(2):1627–1632, 2020.
- Sanjay P Bhat and Dennis S Bernstein. A topological obstruction to continuous global stabilization of rotational motion and the unwinding phenomenon. *Systems & control letters*, 39(1):63–70, 2000.
- Jennie Cochran and Miroslav Krstic. Nonholonomic source seeking with tuning of angular velocity. *IEEE Transactions on Automatic Control*, 54(4):717–731, 2009.
- Jan De Priester, Ricardo G. Sanfelice, and Nathan Van De Wouw. Hysteresis-based rl: Robustifying reinforcement learning-based control policies via hybrid control. In *2022 American Control Conference (ACC)*, pages 2663–2668, 2022. doi: 10.23919/ACC53348.2022.9867627.
- Jan De Priester, Zachary Bell, Prashant Ganesh, and Ricardo Sanfelice. Multihyrl: Robust hybrid rl for obstacle avoidance against adversarial attacks on the observation space. In *Reinforcement Learning Conference*, 2024.
- Sarah Dean, Nikolai Matni, Benjamin Recht, and Vickie Ye. Robust guarantees for perception-based control. In *Learning for Dynamics and Control*, pages 350–360. PMLR, 2020.
- Dieter Fox, Wolfram Burgard, and Sebastian Thrun. The dynamic window approach to collision avoidance. *IEEE Robotics & Automation Magazine*, 4(1):23–33, 1997.
- Dieter Fox, Wolfram Burgard, and Sebastian Thrun. Markov localization for mobile robots in dynamic environments. *Journal of artificial intelligence research*, 11:391–427, 1999.
- Adam Francis, Shuai Li, Christian Griffiths, and Johann Sienz. Gas source localization and mapping with mobile robots: A review. *Journal of Field Robotics*, 39(8):1341–1373, 2022.
- Shuzhi Sam Ge and Yun J Cui. Dynamic motion planning for mobile robots using potential field method. *Autonomous robots*, 13:207–222, 2002.
- Rafal Goebel, Ricardo G. Sanfelice, and Andrew R. Teel. *Hybrid Dynamical Systems: Modeling, Stability, and Robustness*. Princeton university press, Princeton (N.J.), 2012. ISBN 978-0-691-15389-6.
- Oussama Khatib. Real-time obstacle avoidance for manipulators and mobile robots. *The international journal of robotics research*, 5(1):90–98, 1986.
- Steven M LaValle. *Planning algorithms*. Cambridge university press, 2006.
- Tyrell Lewis and Kiran Bhaganagar. A comprehensive review of plume source detection using unmanned vehicles for environmental sensing. *Science of the Total Environment*, 762:144029, 2021.

- Achim Lilienthal and Tom Duckett. Building gas concentration gridmaps with a mobile robot. *Robotics and Autonomous Systems*, 48(1):3–16, 2004.
- Christopher G Mayhew and Andrew R Teel. On the topological structure of attraction basins for differential inclusions. *Systems & Control Letters*, 60(12):1045–1050, 2011.
- Hans P Moravec. The stanford cart and the cmu rover. *Proceedings of the IEEE*, 71(7):872–884, 1983.
- Alejandro Murillo-Gonzalez and Jorge I Poveda. Data-assisted vision-based hybrid control for robust stabilization with obstacle avoidance via learning of perception maps. In *2022 American Control Conference (ACC)*, pages 886–892. IEEE, 2022.
- Robin R Murphy. Activities of the rescue robots at the world trade center from 11-21 september 2001. *IEEE Robotics & Automation Magazine*, 11(3):50–61, 2004.
- Jorge I Poveda, Mouhacine Benosman, Andrew R Teel, and Ricardo G Sanfelice. Robust coordinated hybrid source seeking with obstacle avoidance in multivehicle autonomous systems. *IEEE Transactions on Automatic Control*, 67(2):706–721, 2021.
- Andrew R Russell. *Odour detection by mobile robots*, volume 22. World Scientific, 1999.
- Ricardo G Sanfelice, Michael J Messina, S Emre Tuna, and Andrew R Teel. Robust hybrid controllers for continuous-time systems with applications to obstacle avoidance and regulation to disconnected set of points. In *2006 American Control Conference*, pages 6–pp. IEEE, 2006.
- Roland Siegwart, Illah Reza Nourbakhsh, and Davide Scaramuzza. *Introduction to autonomous mobile robots*. MIT press, 2011.
- Karen Simonyan and Andrew Zisserman. Very deep convolutional networks for large-scale image recognition. In *3rd International Conference on Learning Representations*, 2015.
- Velimir Todorovski and Miroslav Krstic. Practical prescribed-time seeking of a repulsive source by unicycle angular velocity tuning. *Automatica*, 154:111069, 2023.
- Ao Wang, Hui Chen, Lihao Liu, Kai Chen, Zijia Lin, Jungong Han, and Guiguang Ding. Yolov10: Real-time end-to-end object detection. *arXiv preprint arXiv:2405.14458*, 2024.
- Chunlei Zhang, Daniel Arnold, Nima Ghods, Antranik Siranosian, and Miroslav Krstic. Source seeking with non-holonomic unicycle without position measurement and with tuning of forward velocity. *Systems & control letters*, 56(3):245–252, 2007.
- Yian Zhao, Wenyu Lv, Shangliang Xu, Jinman Wei, Guanzhong Wang, Qingqing Dang, Yi Liu, and Jie Chen. Detrs beat yolos on real-time object detection. In *Proceedings of the IEEE/CVF Conference on Computer Vision and Pattern Recognition*, pages 16965–16974, 2024.
- Xizhou Zhu, Weijie Su, Lewei Lu, Bin Li, Xiaogang Wang, and Jifeng Dai. Deformable detr: Deformable transformers for end-to-end object detection. In *International Conference on Learning*, 2021.